Published in final edited form as:
Biochemistry. 2013 April 16; 52(15): 2556–2564. doi:10.1021/bi400146c.

Mutational Effects on the Folding Dynamics of a Minimized Hairpin‡

Michele Scian, **Irene Shu**, **Katherine A. Olsen**, **Khalil Hassam**, and **Niels H. Andersen**
Department of Chemistry, University of Washington, Seattle WA 98195

Abstract

The fold stabilities and folding dynamics of a series of mutants of a model hairpin, KTW-NPATGK-WTE (HP7), are reported. The parent system and the corresponding DPATGK loop species display sub-μs folding time constants. The mutational studies revealed that ultrafast folding requires both some pre-structuring of the loop and a favorable interaction between the chain termini at the transition state. In the case of YY-DPETGT-WY, another sub-μs folding species [Davis, C. M.; Xiao, S.; Raleigh, D. P.; Dyer, R. B. (2012) *J. Am. Chem. Soc. 134*, 14476–14482], a hydrophobic cluster provides the latter. In the case of HP7, the Coulombic interaction between the terminal NH_3^+ and CO_2^- units provides this; a C-terminal Glu to amidated Ala mutation results in a 5-fold folding rate retardation. The effects of mutations within the reversing loop indicate the balance between loop flexibility (favoring fast conformational searching) and turn-formation in the unfolded state is a major factor in determining the folding dynamics. The –NAAAKX- loops examined display no detectable turn formation propensity in other hairpin constructs, but do result in stable analogs of HP7. Peptide KTW-NAAAKK-WTE displays the same fold stability as HP7 but both the folding and unfolding time constants are greater by a factor of 20.

The mechanism by which an initially unstructured polypeptide sequence reaches its native structure circumventing the Levinthal paradox[1] is still controversial. It has been suggested that proteins could avoid searching through all possible conformations by taking specific folding pathways. In the diffusion-collision and the nucleation models[2–4] of protein folding, stepwise rapid formation of local secondary structures drives the folding. Hydrophobic collapse followed by the acquisition of secondary structure and tertiary packing interactions is an alternative model.[5] The structural elements, or "foldons",[6,7] that collide and coalesce to form a protein's tertiary structure must possess the potential to fold to some extent due to strictly local interactions. Helices, local hydrophobic clusters and β-hairpins are potential foldons. In the Dill's zipping-assembly view of protein folding[8–10], multiple foldon condensation pathways are proposed to accelerate protein folding, but conformational searching is still the ultimate speed limit[10] of protein folding.

The frequent observation, for β-sheet proteins, that one β-hairpin is formed before or at the folding transition state[11–20] is evidence for hairpin involvement in nucleation-condensation pathways[21–26]. As a result, there have been efforts to design β-hairpins for dynamics studies

‡This is paper #2 in the series "Elucidating Polypeptide Folding Dynamics by ^{1}H NMR"; paper #1 of the series is citation #28.

*CORRESPONDING AUTHOR. Telephone: 1-(206)-543-7099. andersen@chem.washington.edu.

Supporting Information. More detailed methods descriptions, fold populations (χ_F) from NMR shifts (Table S1), folding and unfolding rates obtained using a single temperature invariant δ_{folded} value of W3-Hε3 (Table S4) and with a temperature dependent δ_{folded} (Table S2), exchange broadenings measured at 500 and 750 MHz (Table S5), correlations between mutational thermodynamic and dynamics changes (Table S3, Figures S4 & S5), and chemical shift melting curves (Figure S1 & S2) for some of the peptides examined. This material is available free of charge via the Internet at http://pubs.acs.org.

outside of the protein context. Experimental measures of $1/k_F$ for non-cyclic β-hairpins at 280 – 298 K have been in the 0.8 – 52 μs range [27–31]; but, contrarily, faster rates ($1/k_F$ = 40 – 140 ns) have been reported for three and four-stranded sheet models[32–34]. In the case of the faster folding double and triple hairpins, Gai and co-workers[33,34] have suggested that the rapid folding observed may reflect multiple pathways to the folded state or downhill folding.

A number of reports have revealed a relationship between the stability of a β-hairpin and the turn-forming propensity of the loop region[35–38]. Moreover, effects of loop length[37,39–42], stabilizing cross-strand interactions[37,42–48], and attractive Coulombic effects between the oppositely charged chain termini[49–52] have also been noted. The influence of these factors on folding rates remains incompletely understood. There have been studies that report an increase in folding rate for reversing loop region mutations that increase the "turn propensity"[29,30,32–34], but other studies[28,41] supported a model for β-hairpin folding in which the rate-limiting step is the loop search process required to establish a near-native cross-strand hydrophobic cluster without prior formation of a well-defined native turn. A recent publication[53] indicates that a choice between these two mechanisms remains elusive for a hairpin with a topology similar to that of the peptides reported herein.

Analogs of the C-terminal hairpin (GB1p) of the B1 domain of protein G,[54,55] including "trpzip" hairpins[56], have played a prominent role in hairpin dynamics studies[28,29,57]. Indeed, fluorescence monitored T-jump experiments[57] on GB1p were the basis for the original hairpin zipper folding mechanism. Our NMR relaxation studies[28] revised $1/k_F$ at 298 K for GB1p from 6 μs to 20 μs; in large part, as a result of a change in the estimated folding equilibrium constant. Recalculating the fluorescence monitored T-jump data using our K_F value brings the two folding time measures ($1/k_F$) to within experimental error (± 2 μs). The folding dynamics data for GB1p and related peptides appear in Table 1.

Loop optimization (GB1m2 *versus* GB1p) increases the stability of the hairpin fold by 4.5 kJ/mol;[51] this result arising exclusively from an increased folding rate. Based on data reported by Du *et al.*[29], the even larger fold stability increase (≥ 7.5 kJ/mol) associated with Trp/Trp interactions in trpzip4 is largely a reflection of retarded unfolding rather than an increase in the folding rate constant. Two loop mutations (D7P and K10G), each of which increase fold stability, have quite different effects on folding dynamics: the D7P mutation increases k_F, and decreases k_U,[28] while the K10G mutation increases both rates dramatically[58]. It would appear that loop configurational entropy considerations (*e.g.* Gly *vs.* Pro content changes), rather than just changes in the net thermodynamic stability, can be a factor in hairpin dynamics. The GB1m3 *versus* GB1m2 comparison in Table 1 indicates that the hairpin stabilization associated with replacing a repulsive Coulombic interaction near the chain termini (E2/E16) with attractive K/E interactions is largely the result of a 2-fold increase in the folding rate. Given the remoteness from the turn loci, we suggested[28] that this was difficult to rationalize by a "zippering" from the turn mechanism of hairpin folding. Subsequent studies have confirmed hairpin stability enhancement due to attractive Coulombic interactions between the charges at the extreme termini of this series of peptides[52]. The last entry in Table 1, CLN025, is a peptide with the same turn geometry that has been reported to be an ultrafast folding system[53]. In the CLN025 study, it was concluded that neither the zipper mechanism nor the hydrophobic collapse mechanism could completely rationalize the result and it was suggested that hydrophobic interactions between the terminal aromatic groups lead to a pre-collapsed structure. In the present paper, we present hairpin dynamics data from NMR relaxation measurements[28,59–62] for a wide range of strand-terminal and loop mutations of peptide HP7[63] to elucidate the hairpin formation pathways. Mutations at the chain termini and a wide range of mutations in the NPATGK loop, which dramatically altered the loop entropy, are tolerated and do not alter the folded state geometry. These mutations do alter the folding equilibrium and provide, as a result,

measures of the effects of both loop and strand mutations on fold stability as well as folding and unfolding rates.

EXPERIMENTAL PROCEDURES

Materials

With the exception of (E12A-NH_2)-HP7, the analogs were synthesized on an Applied Biosystem 433A synthesizer employing standard Fmoc solid-phase peptide synthesis methods. Wang resin preloaded with the C-terminal amino acid in the synthesis provided an unprotected C-terminus upon cleaving. HP7 (KTW-NPATGK-WTE) analogs prepared specifically for this study replaced NPATGK with NGATGK, NPGTGK, NGGTGK, NAAAGK, NAAAKT, NAAAKK, and NAAAKG. For (E12A-NH_2)-HP7, a Rink-amide resin provided a C-terminal amide function upon cleaving.

Additional peptides were prepared to ascertain, in other hairpin contexts, the turn propensities of NPATGK, NAAAGK and NAAAKK with and without the turn-flanking Trp residues. These included KKLWVS-NPATGK-KIWVSA and KKLWVS-NAAAKK-KIWVSA. Fold stability data for these and other constructs appear in the Supporting Information.

Peptides were cleaved using 95 % trifluoroacetic acid (TFA), with 2.5 % triisopropylsilane (TIS) and 2.5 % water. The cleavage product was then purified using reverse-phase HPLC on a Varian C_{18} preparatory-scale column with a water (0.1 % TFA)/acetonitrile (0.085 % TFE) gradient. Collected fractions were then lyophilized and their identity and molecular weight confirmed on a Bruker Esquire ion trap mass spectrometer. In some cases, an additional HPLC purification using a C_8 column with water (0.1 % TFA)/acetonitrile (0.085 % TFE) gradient or a C_4 column with water (0.1 % TFA)/methanol (0.085 % TFE) gradient was required to obtain peptide samples meeting our purity criteria by NMR analysis. All the other HP7 mutants were available from previous studies[63]; these were re-purified prior to an additional determination of the CD and NMR melts as well as NMR linewidths. The structures were fully supported by mass spectrometry with the NMR assignments confirming the sequence and purity. The thermodynamic stability data from CD and NMR studies of the HP7-related peptides are given in Table S1 (Supporting Information).

NMR Spectroscopy

All NMR spectra were collected on Bruker DRX-500 or DMX-750 spectrometers. Peptide resonances were assigned through a combination of 2D-TOCSY and NOESY experiments with WATERGATE[64] solvent suppression. The former employed a 60 ms MLEV-17 spinlock[65] and the latter a 150 ms mixing time. The samples for 2D spectra consisted of 1 – 1.5 mM peptide in buffered water (20 mM or 50 mM phosphate buffer, pH 6.0) with 10 % D_2O. Sodium 2,2-dimethyl-2-silapentane-5-sulfonate (DSS) was used as the internal chemical shift reference and set to 0 ppm under all conditions independent of temperature and phosphate buffer concentration.

For NMR linewidth studies and additional melting data, the peptides were deuterium-exchanged by repeated lyophilization from D_2O and ^{1}H-1D spectra (512 scans acquired at a resolution of 32 K and 64 K points for the 500 MHz and 750 MHz spectrometers, respectively) were collected with 0.6 – 1 mM peptide concentrations in 20 mM or 50 mM pH 6.0 phosphate buffered 99.9% D_2O.

Folding/Unfolding Equilibrium Measurements

Diagnostics of folding for peptide HP7 have already been defined. Expectations based on the pattern of backbone *CSD* values for hairpins[66] are that the (S ± even) Hα and the (S ± odd) H_N should be downfield by circa 1 ppm at 100 % folding (see Figure 1 for the labeling scheme); in HP7 a number of these are modified by ring current effects. It has also been established that the [4:6]-hairpin loop has diagnostic *CSD*s, upfield shifts for G8α (T4), $T3H_N$ and (S + 1) H_N. Based on the folding thermodynamics parameters for HP7,[63] the $CSD_{100\%}$ values for these and key sites that experience ring current shifts have been established. These are detailed in the Supporting Information.

Extracting Folding/Unfolding Rate Constants from Exchange Broadening Data

This NMR method relies on the measurement of exchange broadening (Δ^{ex}). In the case of folded/unfolded state exchanges that occur in the < 100 μs range, where the probe signal will occur at the population-averaged chemical shift, the relationship between linewidth (Δ^{obs}), the exchange rates, and the chemical shift difference ($\Delta\nu$) between the states is given by eq 1,

$$\Delta^{ex}=\Delta^{obs}-\Delta^{0}=4\pi\tau_{ex}\chi_F\chi_U(\Delta\upsilon)^2 \quad (1)$$

where χ_F is the mole fraction of the folded state ($K_F = \chi_F/\chi_U$), Δ^0 is the "intrinsic" linewidth expected in the absence of exchange broadening, and $\tau_{ex} = (k_F + k_U)^{-1}$.

For hairpins and other peptide folds that are incompletely populated under accessible conditions, defining fully-folded structuring shifts ($CSD_{100\%}$) and whether they may have some residual temperature dependence stands as the greatest potential source of error in dynamic NMR folding rate determinations. Once these have been defined, however, the NMR method has the distinct advantage that the equilibrium constant at any temperature can be derived from the observed chemical shift for the probe (eq 2).

$$\chi_F=(\delta_{obs}-\delta_{coil})/CSD_{100\%} \quad (2)$$

Further details concerning how we extract Δ^{ex} from lineshape differences between two first order doublets with the same coupling constant have been published previously[28] and their specific implementation in the present case appears in the Supporting Information.

Measurements at two field strengths provide a test of an inherent assumption in the method, that Δ^{ex} can be attributed exclusively to exchange broadening due to the folded/unfolded equilibrium. Exchange broadening due to this mechanism should be proportional to $(\Delta\nu)^2$; thus, the calculated Δ^{ex} should be 2.25 times as large at 750 *versus* 500 MHz. For Δ^{ex} values greater than 1.2 Hz at 500 MHz, this condition is met within experimental error (Table S3, Supporting Information). When Δ^{ex} is small (< 2.5 Hz at 750 MHz), we employ only the value determined at 750 MHz for rate calculations.

Folding rate constants are derived using eq 3. With the folding equilibrium constant established, this also provides the unfolding rate.

$$k_F=4\pi\chi_U(\chi_F)^2(\Delta\upsilon)^2(\Delta^{ex})^{-1} \quad (3)$$

Eq 3, which applies near the fast exchange limit, was reported in 1959 by Piette and Anderson[67] and applied to hairpin dynamics[68] in 1999, when it was used to extract upper

limits for 3-stranded sheet formation timescales. We have previously established the conditions required for the application of the eq 3;[28] all of the systems examined herein meet those conditions. In order to obtain error estimates for k_F, we use χ_U values based on alternative *CSD* values, one based on a single common value for the chemical shift of the Trp Hε3 probe in the folded state independent of loop mutations, and two others based on the $CSD_{100\%}$ values (and δ_F temperature dependencies) derived from Table S1.

RESULTS

The backbone conformation, and the particular edge-to-face (EtF) packing motif of the indole rings in the turn-flanking Trp residues, observed in the β-hairpins examined herein is shown in Figure 2. The EtF aromatic interaction results in a dramatic (> 2.2 ppm) upfield structuring shift for the N-terminal Trp Hε3 resonance (W3-Hε3) due to the ring current effects of the other Trp. The linewidths of this shifted resonance provide the dynamics data.

The Hε3 resonance of the Trp at the C-terminus experiences virtually no structuring shift, and thus, is an ideal internal reference for establishing intrinsic broadening effects (Δ^0). We observe significant differential broadening at the upfield shifted W3-Hε3 resonance of hairpins with this motif, see Figure 3, *vide infra*.

Verification of two-state folding and accurate $\Delta\nu$ values are the key requirements for extracting meaningful rates by the NMR linewidth method we employ. The use of several local probes represents a stringent test for two-state folding. Chemical shifts provide a powerful tool for detecting partially folded states under equilibrium melting conditions. For non-2-state melting behavior, some sequence segments of the peptide would be expected to show structuring shifts (native-like or reflecting an alternative structure) while others would be in a statistical coil conformation, leading to different local melting curves depending on the probe location[28,41,66,69,70]. We employed eight backbone proton sites for measuring the fraction folded values (χ_F) of the hairpins. Five of these monitor β-strand alignment, the other three indicate the extent of turn formation. The agreement between these folding measures for distinct sub-structural elements supports a two-state unfolding mechanism for all of the species examined (Supporting Information). The melting curves for each of these proton sites revealed that all of them displayed the same fractional degree of unfolding on warming; strong evidence against the formation of partially melted intermediates and a downhill folding scenario.

Since the upfield W3-Hε3 resonance provides both the shift data giving the extent of folding (χ_F) and the linewidths that afford the folding dynamics, the accuracy of extrapolated 100 % folded value for this site (and its temperature dependence) in each peptide was a major concern. The extrapolated 100 % folded *CSD*s at 280 K for the HP7 series of peptides ranged from −2.39 to −2.64 ppm (Supporting Information). As has been observed in other studies[71–73], Hε3 ring current shifts in cross-strand Trp/Trp units decrease at higher temperatures. This was incorporated in our dynamics analysis as a temperature dependent value for the fully-folded chemical shift of W3-Hε3. For the present set of analogs two values were required for the analysis, either $\delta_F = 5.15 + 0.004(T-280)$ or $\delta_F = 4.98 + 0.005(T-280)$. The latter applied to analogs with extensive mutations in the NPATGK loop. Chemical shift melting curves of W3-Hε3 resonance for all of the peptides in D_2O (the medium employed for the NMR lineshape analyses) that support the use of these equations appear in Supporting Figures S1 & S2.

One advantage of using chemical shift as a probe of folding is that this method is insensitive to partial aggregation of the sample at elevated temperature, a common problem in thermal denaturation studies. Aggregation dynamics are much slower than conformer

interconversion with the broad signals for the aggregate not averaged in with those of the monomeric state. However, even under these conditions the monomer/aggregate interconversion can result in broadening of the monomer signals but the resulting linewidth increment due to exchange with an aggregate does not scale with $\Delta\nu$. Rapid exchange between the monomeric folded state and the unfolded ensemble will result in Δ^{ex} values that are proportional to $(\Delta\nu)^2$ and, thus, to (field-strength)^2. In every case, the Δ^{ex}-ratio values derived for HP7 analogs at 500 *versus* 750 MHz are in the expected ratio (2.25): 2.33 ± 0.20 (n = 24), see Table S5.

The resonances for the two Trp Hε3 sites were resolved in all of the analogs examined with only the upfield W3 site displaying line broadening. Figure 3 illustrates a large difference in Hε3 linewidths observed for two HP7 systems that have essentially the same fold stability and very similar melting behavior.

For dynamics analyses, we always assumed the same coil value (7.58 ppm) for Trp Hε3 but employed the alternative temperature-dependent δ_{folded} values given above. In an alternate analysis, we assumed a common δ_{folded} = 5.10 ppm, independent of loop residue or chain termini mutations. As a rule, the Arrhenius plots derived using the temperature dependent $CSD_{100\%}$ value provided a more nearly linear plot for ln k_U. The key fold stabilities (as ΔG_U) and folding and unfolding rates appear in Table 2. Table S2 (Supporting Information) provides data at additional temperatures, complementary data measured at 500 MHz, and includes the χ_F values for each entry.

Accurate dynamics data are available over a 6 kJ/mol range ($\Delta\Delta G_U$) of fold stabilities at 300 K. The range of both folding and unfolding rates is larger, 9 kJ/mol in RT(ln k) units; throughout, Arrhenius behavior is observed. In all cases, the plot of ln k_U *versus* reciprocal temperature is linear within experimental error. The slopes of the Arrhenius plots for k_U are quite similar, reflecting a (2.5 ± 0.2)-fold rate increase for a 10 °C temperature increment. Representative Arrhenius plots appear in Figure 4 and the Supporting Information. For examining the correlation between thermodynamic stability and dynamics effects of mutations, we compare $\Delta\Delta G_U$ and Δ(ln k); these are tabulated for single site loop mutations in the Supporting Information (Table S3).

DISCUSSION

The NPATGK loop of HP7 was based[51] on location-specific residue statistics for [4:6]-hairpins in proteins. This sequence has, subsequently been successfully employed in a number of hairpin and three-stranded constructs[66,74]. A similar analysis led Honda and co-workers to the DPETGT turn sequence that appears in chignolin[75] and further optimized hairpins[76]. The present study serves to confirm that the key features of this turn sequence are aryl-Asx-XXXGX-aryl, with the flanking aromatic residues providing significant stability. This is borne out by the effects of single site residue mutations within this sequence in HP7 analogs (Table S3); an N4A mutation was highly destabilizing (folding rates could not be determined), with the G8A mutation having the largest effect on the folding rate (a 7-fold retardation), with a smaller reduction observed for k_U. These results were, to some extent expected since G8 has φ/ψ = +94/47 ° in the HP7 NMR structure ensemble[63]. In the case of the NAAAKK loop mutant, we examined the effect of non-native *versus* native introduction of glycine: NAAAKK → NAAAKG ($\Delta\Delta G_U$ = −3.4 kJ/mol, Δln k_F = +0.6, Δln k_U = +2.0) *versus* NAAAKK → NAAAGK ($\Delta\Delta G_U$ = +0.7 kJ/mol, Δln k_F = +1.5, Δln k_U = +1.2). The introduction of glycines at positions other than the “native” one (G8) is destabilizing and results in enhanced melting, but the effects on the dynamics are not uniform (Table S3). In the case of NAAAKK → NAAAKG, the glycine insertion increases both the folding and unfolding rate (see Figure S6, Supporting Information). With a decrease in ΔG_U in this case,

the accelerated folding can, in our opinion, only be attributed to a more rapid conformational search for the fold-stabilizing indole/indole geometry at the ends of a more flexible loop upon introducing a Gly unit.

Turning to the specific questions raised in the introduction concerning the factors that govern hairpin formation rates, the present HP7 analog data provide insights into three features: 1) the effects of Coulombic interactions near the chain termini, 2) the correlation between folding rates and thermodynamic stability, and 3) the effects of loop flexibility *versus* intrinsic conformational preferences. Arrhenius plot comparisons (Figures 4) provide data regarding the Coulombic effect; these probe the effects of the interaction of both oppositely charged sidechains near the chain termini and of the N-terminal NH_3^+ and the C-terminal backbone carboxylate on fold stability and dynamics.

There are also many examples in the literature[45–50,63] in which C-terminal carboxylate protonation reduce hairpin fold stability. In the present study, we examined the effects on folding dynamics in the case of the NAAAKT loop mutant. Carboxylate protonation, as for other HP7 analogs[63], is destabilizing with a 2-fold decrease in the folding rate constant and an acceleration of unfolding.

The chain terminal [K1A,E12A]-HP7 and [E12A-NH_2]-HP7 mutations probe the effects of the interaction of both oppositely charged sidechains near the chain termini and of the N-terminal NH_3^+ and the C-terminal backbone carboxylate on fold stability and dynamics. Replacing the N-terminal Lys and the C-terminal Glu with alanine does not alter the folding rate; the slight decrease in thermodynamic stability associated with this change is due to somewhat accelerated unfolding. This analog retains the attractive interaction between the backbone NH_3^+ and C-terminal CO_2^- units. In contrast, replacing the C-terminal Glu with amidated alanine, which remove this interaction, results in a significant (5-fold) decrease in the folding rate with essentially no change in the unfolding rate constant. This comparison suggests that the fold-favoring Coulombic effect reflects folding acceleration due to the charges at the backbone termini with less contribution from oppositely charged sidechain functions. There are cases in the literature[52,63] in which N-terminal acetylation has been demonstrated to decrease hairpin fold stability. These may reflect the same phenomenon.

Substantial folding rate acceleration due to an attractive Coulombic interaction between the extreme termini of the structure would require, with a zippering from the turn mechanism, a late transition state with nearly complete hairpin formation. The alternative is a collapsed structure including Coulombic association between the termini as an early intermediate in folding with cross-strand H-bonding and the formation of the stabilizing turn-flanking Trp/Trp interactions as somewhat later events in the folding pathway.

Turning to the second question, the correlation between folding rates and thermodynamic stability, this has been studied extensively in other systems, particularly proteins. A common feature observed in prior reports of hairpin dynamics comparisons over turn replacements and turn site mutations has been an increased folding rate for turn sequences with an enhanced turn-forming propensity[29,30]. With the extensive studies of replacements of the SRSSGR reversing loop in the Pin1 WW domain by Kelly and Gruebele[77–79], this conclusion has been extended to protein contexts. Among the single site mutations we examined, NAATGK → NAAAGK ($\Delta\Delta G_U$ = +1.7 kJ/mol, $\Delta \ln k_F$ = −1.2, $\Delta \ln k_U$ = −1.7) is a clear exception to this expected correlation. Slow folding, coupled with surprisingly high thermodynamic stability, was observed for all of the NAAAXX loop species examined. For the NP^5AT^7GK reversing loop, the P5A and T7A mutations each decreased fold stability and the folding rate constant, the double mutation resulted in a folding rate retardation that was slighter greater than the sum of the effects of the two individual

mutations but this was coupled with significant fold stabilization. The NAAAKK loop species is the slowest folding species examined, even though it has the same fold stability as the "optimized" NPATGK loop species (HP7). The NMR spectra that provided the folding dynamics for these two species appear in Figure 3. At 300 K, both are 89 ± 1 % folded in D_2O; the exchange broadening observed is 1.7 and 34 Hz (at 750 MHz), respectively, corresponding to a 20-fold difference in both the folding and unfolding rates constants.

To explore potential differences between the "optimized" NPATGK reversing loop and the NAAAXX loops, we examined them as a replacement for β-turn sequences (*e.g.* XNGK and X-(D-Pro)-GK, X = S,V, or I) in hairpins and 3-stranded sheet models with and without the turn-flanking Trp/Trp-pair (see Supporting Information). A turn-flanking aryl/aryl pair, also a feature of the GB1 peptide[54–56], is important for high fold stability with both sequences. However, the NAAAKK (and other NAAAXX) sequence cannot replace favorable β-turns in the absence of the flanking aryl/aryl pair while the NPATGK sequence does appear to have an "intrinsic" chain reversing propensity[74,80].

Turning to loop search and stiffness considerations, loop contact time studies have established that Pro has the most dramatic rate retarding effect in loop conformational searches while the increased flexibility of Gly can decrease loop-end contact times[81,82]. With the NPATGK loop sequence, however, a significant level of loop pre-structuring may occur. Loop mutants with the PATG sequence replaced by AAAK should display comparable flexibility, but turn-like conformations appear to be less significant contributors to the unfolded ensemble for the AAAK species. Thus, with both Pro and Gly at their preferred locations in the loop sequence, the folding direction is favored by loop pre-structuring. The observation that unfolding is retarded by the PATG → AAAK change to the same extent as folding, suggests that unfolding proceeds through an enthalpically unfavorable loop conformation for the NAAAK species. For this series of hairpins, there is no apparent correlation between fold stability and the rate of fold formation; rather the data support a role for loop conformational search requirements, including loop flexibility, and the extent to which pre-structuring of the loop is favored by the sequence.

How do these new observations regarding hairpin dynamics fit within the context of other literature observations and current questions concerning protein folding mechanisms? Given the close structural analogies between the HP7 hairpins and CLN025 (YY-DPETGT-WY, T_m = 70°C), this is the first comparison considered here. Although the authors reported[53] the CLN025 dynamics data as relaxation rates rather than specific k_F and k_U values, folding equilibrium constants were also reported; these allow a calculation of $1/k_F$, ~ 190 (298 K) and ~ 115 ns (318 K). The fastest folding times we observed were for our DPATGK and NPATGK loop species were $1/k_F$ = 530 (300 K) and 150 ns (320 K). All of these folding times are faster than the expected[53,83,84] 1-μs speed limit for hairpin formation.

There are some distinctions between the dynamics data for CLN025 and the HP7 analogs. CLN025 displayed a break at 308 K in both the van't Hoff melt analysis and the Arrhenius plot for ln k_R, with probe-dependent kinetics observed in the high temperature region. In the Arrhenius plot, this corresponds to a radically decreased slope at temperatures above the break point, suggesting either no or a very small (< 10 kJ/mol) activation energy. Some of the HP7 analogs display a flattening of the Arrhenius plot for ln k_F; however, we did not extend the studies to high enough temperatures to ascertain whether there are two distinct folding regimes since other evidence suggested that aggregation becomes a competing process at higher temperatures. The unfolding activation energies (*Ea*) for HP7 analogs are relatively constant (69 ± 6 kJ/mol). The *Ea*-values derived from the linear fits to the Arrhenius plots for folding rates in Figures 4 and S6 range from 30 – 50 kJ/mol, values that bracket the ~ 45 kJ/mol value observed for the low-temperature portion of the CLN025

Arrhenius plot. The fastest folding system (the NPATGK loop with “wild-type” strands) has the largest activation energy (~50 kJ/mol) in the folding direction. We view this, in the case of the HP7 systems, as the barrier for an essentially 2-state folding process that includes the formation of the Trp/Trp EtF interaction and some cross-strand H-bonds within a short anti-parallel β-sheet. CLN025 also has an EtF aryl/aryl pair (Y2/W9) but these sidechains, in combination with Y1 and Y10, may represent hydrophobic capping of a turn rather than 2-residue β-strands. This may reduce the extent to which CLN025 is an appropriate model for hairpin folding.

Given the observation of probe-dependent dynamics for CLN025,[53] it will be essential to ascertain whether this is also the case for the HP7 hairpins. Efforts to provide this information are in progress. To date, Trp-fluorescence-monitored T-jump studies (15 – 26 °C) have confirmed the ultrafast folding of the NPATGK loop species, the folding rate retardation associated with the C-terminal Glu to Ala-NH_2 mutation, the slow folding of the NGGTGK loop species, and the even slower folding of two NAAAKX loop species. Since Trp-fluorescence changes may reflect the same structuring transition that determines the ring current shifts used in NMR dynamics, the synthesis of systems with $^{13}C{=}O$ labels at sites that monitor specific H-bond formation within the reversing loops and between the β-strands for T-jump experiments is in progress. These should provide the additional probes needed to ascertain whether there is sequential formation of different structural elements (or strict two-state folding) for these hairpin models. However, it already apparent that this series of HP7 analogs has provided evidence that ultrafast hairpin formation requires both some pre-structuring of the loop and favorable Coulombic interactions between the chain termini. The latter is provided by the backbone NH_3^+/CO_2^- groups. The NPATGK sequence results in loop pre-structuring while a variety of NAAAKX sequences do not, even though stable hairpins result with all of these loop sequences. We anticipate that these sequences in hairpins stabilized with β-capping units at the ends of longer β-strands will provide additional insights into the contribution of loop conformational search times to β-hairpin formation.

Supplementary Material

Refer to Web version on PubMed Central for supplementary material.

Acknowledgments

Funding Sources

This work was supported by grants from the National Science Foundation (CHE0650318 and CHE1152218). M.S. received salary as a post-doctoral research associate on NIH grant GM059658 during some of these studies.

We thank Gurusamy Balakrishnan for providing fluorescence-monitored T-jump data for a number of HP7 analogs that served to validate the NMR lineshape dynamics.

References

1. Levinthal, C. Mossbauer Spectroscopy in Biological Systems. In: Debrunner, P.; Tsibris, JCM.; Munch, E., editors. Mossbauer Spectroscopy in Biological Systems. University of Illinois; Monticello, Illinois: 1969. p. 22-24.
2. Karplus M, Weaver DL. Protein-folding dynamics. Nature. 1976; 260:404–406. [PubMed: 1256583]
3. Wetlaufer DB. Nucleation, rapid folding, and globular intrachain regions in proteins. Proc Natl Acad Sci U S A. 1973; 70:697–701. [PubMed: 4351801]
4. Daggett V, Fersht AR. Is there a unifying mechanism for protein folding? Trends Biochem Sci. 2003; 28:18–25. [PubMed: 12517448]

5. Ptitsyn OB. Protein Folding - Hypotheses and Experiments. J Protein Chem. 1987; 6:273–293.
6. Dill KA, Fiebig KM, Chan HS. Cooperativity in protein-folding kinetics. Proc Natl Acad Sci U S A. 1993; 90:1942–1946. [PubMed: 7680482]
7. Panchenko AR, Luthey-Schulten Z, Wolynes PG. Foldons, protein structural modules, and exons. Proc Natl Acad Sci U S A. 1996; 93:2008–2013. [PubMed: 8700876]
8. Dill KA, Ozkan SB, Weikl TR, Chodera JD, Voelz VA. The protein folding problem: when will it be solved? Curr Opin Struct Biol. 2007; 17:342–346. [PubMed: 17572080]
9. Voelz VA, Dill KA. Exploring zipping and assembly as a protein folding principle. Proteins. 2007; 66:877–888. [PubMed: 17154424]
10. Ghosh K, Ozkan SB, Dill KA. The ultimate speed limit to protein folding is conformational searching. J Am Chem Soc. 2007; 129:11920–11927. [PubMed: 17824609]
11. Matheson RR, Scheraga HA. Method for Predicting Nucleation Sites for Protein Folding Based on Hydrophobic Contacts. Macromolecules. 1978; 11:819–829.
12. Grantcharova VP, Riddle DS, Santiago JV, Baker D. Important role of hydrogen bonds in the structurally polarized transition state for folding of the src SH3 domain. Nat Struct Biol. 1998; 5:714–720. [PubMed: 9699636]
13. Grantcharova VP, Riddle DS, Baker D. Long-range order in the src SH3 folding transition state. Proc Natl Acad Sci U S A. 2000; 97:7084–7089. [PubMed: 10860975]
14. Martinez JC, Serrano L. The folding transition state between SH3 domains is conformationally restricted and evolutionarily conserved. Nat Struct Biol. 1999; 6:1010–1016. [PubMed: 10542091]
15. Kortemme T, Kelly MJ, Kay LE, Forman-Kay J, Serrano L. Similarities between the spectrin SH3 domain denatured state and its folding transition state. J Mol Biol. 2000; 297:1217–1229. [PubMed: 10764585]
16. Walkenhorst WF, Edwards JA, Markley JL, Roder H. Early formation of a beta-hairpin during folding of staphylococcal nuclease H124L as detected by pulsed hydrogen exchange. Protein Sci. 2002; 11:82–91. [PubMed: 11742125]
17. Gruebele M, Wolynes PG. Satisfying turns in folding transitions. Nat Struct Biol. 1998; 5:662–665. [PubMed: 9699621]
18. Martinez JC, Pisabarro MT, Serrano L. Obligatory steps in protein folding and the conformational diversity of the transition state. Nat Struct Biol. 1998; 5:721–729. [PubMed: 9699637]
19. Guo ZY, Thirumalai D. Kinetics of Protein-Folding - Nucleation Mechanism, Time Scales, and Pathways. Biopolymers. 1995; 36:83–102.
20. McCallister EL, Alm E, Baker D. Critical role of beta-hairpin formation in protein G folding. Nat Struct Biol. 2000; 7:669–673. [PubMed: 10932252]
21. Bofill R, Simpson ER, Platt GW, Crespo MD, Searle MS. Extending the folding nucleus of ubiquitin with an independently folding beta-hairpin finger: hurdles to rapid folding arising from the stabilisation of local interactions. J Mol Biol. 2005; 349:205–221. [PubMed: 15876378]
22. Went HM, Jackson SE. Ubiquitin folds through a highly polarized transition state. Protein Eng Des Sel. 2005; 18:229–237. [PubMed: 15857839]
23. Gu H, Kim D, Baker D. Contrasting roles for symmetrically disposed beta-turns in the folding of a small protein. J Mol Biol. 1997; 274:588–596. [PubMed: 9417937]
24. Riddle DS, Grantcharova VP, Santiago JV, Alm E, Ruczinski I, Baker D. Experiment and theory highlight role of native state topology in SH3 folding. Nat Struct Biol. 1999; 6:1016–1024. [PubMed: 10542092]
25. Fersht AR. The sixth Datta Lecture. Protein folding and stability: the pathway of folding of barnase. FEBS Lett. 1993; 325:5–16. [PubMed: 8513892]
26. Neira JL, Fersht AR. An NMR study on the beta-hairpin region of barnase. Fold Des. 1996; 1:231–241. [PubMed: 9079384]
27. Munoz V, Ghirlando R, Blanco FJ, Jas GS, Hofrichter J, Eaton WA. Folding and aggregation kinetics of a beta-hairpin. Biochemistry. 2006; 45:7023–7035. [PubMed: 16752893]
28. Olsen KA, Fesinmeyer RM, Stewart JM, Andersen NH. Hairpin folding rates reflect mutations within and remote from the turn region. Proc Natl Acad Sci U S A. 2005; 102:15483–15487. [PubMed: 16227442]

29. Du D, Zhu Y, Huang CY, Gai F. Understanding the key factors that control the rate of beta-hairpin folding. Proc Natl Acad Sci U S A. 2004; 101:15915–15920. [PubMed: 15520391]
30. Du D, Tucker MJ, Gai F. Understanding the mechanism of beta-hairpin folding via phi-value analysis. Biochemistry. 2006; 45:2668–2678. [PubMed: 16489760]
31. Snow CD, Qiu L, Du D, Gai F, Hagen SJ, Pande VS. Trp zipper folding kinetics by molecular dynamics and temperature-jump spectroscopy. Proc Natl Acad Sci U S A. 2004; 101:4077–4082. [PubMed: 15020773]
32. Chen RP, Huang JJ, Chen HL, Jan H, Velusamy M, Lee CT, Fann W, Larsen RW, Chan SI. Measuring the refolding of beta-sheets with different turn sequences on a nanosecond time scale. Proc Natl Acad Sci U S A. 2004; 101:7305–7310. [PubMed: 15123838]
33. Xu Y, Purkayastha P, Gai F. Nanosecond folding dynamics of a three-stranded beta-sheet. J Am Chem Soc. 2006; 128:15836–15842. [PubMed: 17147395]
34. Xu Y, Bunagan MR, Tang J, Gai F. Probing the kinetic cooperativity of beta-sheet folding perpendicular to the strand direction. Biochemistry. 2008; 47:2064–2070. [PubMed: 18197708]
35. Haque TS, Gellman SH. Insights on beta-hairpin stability in aqueous solution from peptides with enforced type I′ and type II′ beta-turns. J Am Chem Soc. 1997; 119:2303–2304.
36. de Alba E, Jimenez MA, Rico M. Turn residue sequence determines beta-hairpin conformation in designed peptides. J Am Chem Soc. 1997; 119:175–183.
37. Espinosa JF, Munoz V, Gellman SH. Interplay between hydrophobic cluster and loop propensity in beta-hairpin formation. J Mol Biol. 2001; 306:397–402. [PubMed: 11178900]
38. Espinosa JF, Syud FA, Gellman SH. Analysis of the factors that stabilize a designed two-stranded antiparallel beta-sheet. Protein Sci. 2002; 11:1492–1505. [PubMed: 12021448]
39. Gunasekaran K, Ramakrishnan C, Balaram P. Beta-hairpins in proteins revisited: lessons for de novo design. Protein Eng. 1997; 10:1131–1141. [PubMed: 9488138]
40. Blandl T, Cochran AG, Skelton NJ. Turn stability in beta-hairpin peptides: Investigation of peptides containing 3:5 type I G1 bulge turns. Protein Sci. 2003; 12:237–247. [PubMed: 12538887]
41. Dyer RB, Maness SJ, Peterson ES, Franzen S, Fesinmeyer RM, Andersen NH. The mechanism of beta-hairpin formation. Biochemistry. 2004; 43:11560–11566. [PubMed: 15350142]
42. Espinosa JF, Gellman SH. A Designed beta-Hairpin Containing a Natural Hydrophobic Cluster. Angew Chem Int Ed Engl. 2000; 39:2330–2333. [PubMed: 10941081]
43. Constantine KL, Mueller L, Andersen NH, Tong H, Wandler CF, Friedrichs MS, Bruccoleri RE. Structural and Dynamic Properties of a Beta-Hairpin-Forming Linear Peptide. 1 Modeling Using Ensemble-Averaged Constraints. J Am Chem Soc. 1995; 117:10841–10854.
44. de Alba E, Rico M, Jimenez MA. Cross-strand side-chain interactions versus turn conformation in beta-hairpins. Protein Sci. 1997; 6:2548–2560. [PubMed: 9416604]
45. Searle MS, Williams DH, Packman LC. A short linear peptide derived from the N-terminal sequence of ubiquitin folds into a water-stable non-native beta-hairpin. Nat Struct Biol. 1995; 2:999–1006. [PubMed: 7583674]
46. Ramirez-Alvarado M, Blanco FJ, Serrano L. De novo design and structural analysis of a model beta-hairpin peptide system. Nat Struct Biol. 1996; 3:604–612. [PubMed: 8673604]
47. Maynard AJ, Sharman GJ, Searle MS. Origin of beta-hairpin stability in solution: Structural and thermodynamic analysis of the folding of model peptide supports hydrophobic stabilization in water. J Am Chem Soc. 1998; 120:1996–2007.
48. Griffiths-Jones SR, Maynard AJ, Searle MS. Dissecting the stability of a beta-hairpin peptide that folds in water: NMR and molecular dynamics analysis of the beta-turn and beta-strand contributions to folding. J Mol Biol. 1999; 292:1051–1069. [PubMed: 10512702]
49. de Alba E, Blanco FJ, Jimenez MA, Rico M, Nieto JL. Interactions responsible for the pH dependence of the beta-hairpin conformational population formed by a designed linear peptide. Eur J Biochem. 1995; 233:283–292. [PubMed: 7588757]
50. Kiehna SE, Waters ML. Sequence dependence of beta-hairpin structure: comparison of a salt bridge and an aromatic interaction. Protein Sci. 2003; 12:2657–2667. [PubMed: 14627727]

51. Fesinmeyer RM, Hudson FM, Andersen NH. Enhanced hairpin stability through loop design: the case of the protein G B1 domain hairpin. J Am Chem Soc. 2004; 126:7238–7243. [PubMed: 15186161]
52. Huyghues-Despointes BM, Qu X, Tsai J, Scholtz JM. Terminal ion pairs stabilize the second beta-hairpin of the B1 domain of protein G. Proteins. 2006; 63:1005–1017. [PubMed: 16470585]
53. Davis CM, Xiao S, Raleigh DP, Dyer RB. Raising the Speed Limit for beta-Hairpin Formation. J Am Chem Soc. 2012; 134:14476–14482. [PubMed: 22873643]
54. Blanco FJ, Rivas G, Serrano L. A short linear peptide that folds into a native stable beta-hairpin in aqueous solution. Nat Struct Biol. 1994; 1:584–590. [PubMed: 7634098]
55. Kobayashi, N.; Endo, S.; Munekata, E. Conformational study on the IgG binding domain of protein G. In: Yanaikara, N., editor. Peptide Chemistry 1992. ESCOM Leiden; The Nederland, Shizuoka, Japan: 1993. p. 278-281.
56. Cochran AG, Skelton NJ, Starovasnik MA. Tryptophan zippers: stable, monomeric beta -hairpins. Proc Natl Acad Sci U S A. 2001; 98:5578–5583. [PubMed: 11331745]
57. Munoz V, Thompson PA, Hofrichter J, Eaton WA. Folding dynamics and mechanism of beta-hairpin formation. Nature. 1997; 390:196–199. [PubMed: 9367160]
58. Olsen, KA. PhD thesis. University of Washington; 2006. NMR Studies Reveal the Kinetics and Thermodynamics of Hairpin Formation.
59. Myers JK, Oas TG. Preorganized secondary structure as an important determinant of fast protein folding. Nat Struct Biol. 2001; 8:552–558. [PubMed: 11373626]
60. Arora P, Oas TG, Myers JK. Fast and faster: a designed variant of the B-domain of protein A folds in 3 microsec. Protein Sci. 2004; 13:847–853. [PubMed: 15044721]
61. Huang GS, Oas TG. Submillisecond folding of monomeric lambda repressor. Proc Natl Acad Sci U S A. 1995; 92:6878–6882. [PubMed: 7624336]
62. Wang M, Tang Y, Sato S, Vugmeyster L, McKnight CJ, Raleigh DP. Dynamic NMR line-shape analysis demonstrates that the villin headpiece subdomain folds on the microsecond time scale. J Am Chem Soc. 2003; 125:6032–6033. [PubMed: 12785814]
63. Andersen NH, Olsen KA, Fesinmeyer RM, Tan X, Hudson FM, Eidenschink LA, Farazi SR. Minimization and optimization of designed beta-hairpin folds. J Am Chem Soc. 2006; 128:6101–6110. [PubMed: 16669679]
64. Piotto M, Saudek V, Sklenar V. Gradient-tailored excitation for single-quantum NMR spectroscopy of aqueous solutions. J Biomol NMR. 1992; 2:661–665. [PubMed: 1490109]
65. Braunschweiler L, Ernst RR. Coherence Transfer by Isotropic Mixing - Application to Proton Correlation Spectroscopy. J Magn Reson. 1983; 53:521–528.
66. Fesinmeyer RM, Hudson FM, Olsen KA, White GW, Euser A, Andersen NH. Chemical shifts provide fold populations and register of beta-hairpins and beta-sheets. J Biomol NMR. 2005; 33:213–231. [PubMed: 16341751]
67. Piette LH, Anderson WA. Potential Energy Barrier Determinations for Some Alkyl Nitrites by Nuclear Magnetic Resonance. J Chem Phys. 1959; 30:899–908.
68. de Alba E, Santoro J, Rico M, Jimenez MA. De novo design of a monomeric three-stranded antiparallel beta-sheet. Protein Sci. 1999; 8:854–865. [PubMed: 10211831]
69. Ferguson N, Sharpe TD, Schartau PJ, Sato S, Allen MD, Johnson CM, Rutherford TJ, Fersht AR. Ultra-fast barrier-limited folding in the peripheral subunit-binding domain family. J Mol Biol. 2005; 353:427–446. [PubMed: 16168437]
70. Ferguson N, Sharpe TD, Johnson CM, Schartau PJ, Fersht AR. Structural biology: analysis of “downhill” protein folding. Nature. 2007; 445:E14–15. discussion E17–18. [PubMed: 17301742]
71. Kier BL, Andersen NH. Probing the lower size limit for protein-like fold stability: ten-residue microproteins with specific, rigid structures in water. J Am Chem Soc. 2008; 130:14675–14683. [PubMed: 18842046]
72. Eidenschink L, Kier BL, Huggins KN, Andersen NH. Very short peptides with stable folds: building on the interrelationship of Trp/Trp, Trp/cation, and Trp/backbone-amide interaction geometries. Proteins. 2009; 75:308–322. [PubMed: 18831035]

73. Kier BL, Shu I, Eidenschink LA, Andersen NH. Stabilizing capping motif for beta-hairpins and sheets. Proc Natl Acad Sci U S A. 2010; 107:10466–10471. [PubMed: 20484672]
74. Shu, I.; Scian, M.; Kier, BL.; Williams, DH.; Andersen, NH. Tryptophan interactions that stabilize folding motifs: a guide to placement, dynamics, and optimizing fold stabilization. In: Lebl, M.; Meldal, M.; Jensen, KJ.; Hoeg-Jensen, T., editors. Proceedings of the 31st European Peptide Symposium. European Peptide Society; 2010. p. 614-615.
75. Honda S, Yamasaki K, Sawada Y, Morii H. 10 residue folded peptide designed by segment statistics. Structure. 2004; 12:1507–1518. [PubMed: 15296744]
76. Honda S, Akiba T, Kato YS, Sawada Y, Sekijima M, Ishimura M, Ooishi A, Watanabe H, Odahara T, Harata K. Crystal structure of a ten-amino acid protein. J Am Chem Soc. 2008; 130:15327–15331. [PubMed: 18950166]
77. Nguyen H, Jager M, Kelly JW, Gruebele M. Engineering a beta-sheet protein toward the folding speed limit. J Phys Chem B. 2005; 109:15182–15186. [PubMed: 16852923]
78. Liu F, Du D, Fuller AA, Davoren JE, Wipf P, Kelly JW, Gruebele M. An experimental survey of the transition between two-state and downhill protein folding scenarios. Proc Natl Acad Sci U S A. 2008; 105:2369–2374. [PubMed: 18268349]
79. Fuller AA, Du D, Liu F, Davoren JE, Bhabha G, Kroon G, Case DA, Dyson HJ, Powers ET, Wipf P, Gruebele M, Kelly JW. Evaluating beta-turn mimics as beta-sheet folding nucleators. Proc Natl Acad Sci U S A. 2009; 106:11067–11072. [PubMed: 19541614]
80. Shu, I. PhD Thesis. University of Washington; Seattle, WA: 2011. Thermodynamics and Kinetics of beta-Sheet Folding Models.
81. Krieger F, Fierz B, Bieri O, Drewello M, Kiefhaber T. Dynamics of unfolded polypeptide chains as model for the earliest steps in protein folding. J Mol Biol. 2003; 332:265–274. [PubMed: 12946363]
82. Krieger F, Moglich A, Kiefhaber T. Effect of proline and glycine residues on dynamics and barriers of loop formation in polypeptide chains. J Am Chem Soc. 2005; 127:3346–3352. [PubMed: 15755151]
83. Kubelka J, Hofrichter J, Eaton WA. The protein folding “speed limit”. Curr Opin Struct Biol. 2004; 14:76–88. [PubMed: 15102453]
84. Dyer RB. Ultrafast and downhill protein folding. Curr Opin Struct Biol. 2007; 17:38–47. [PubMed: 17223539]

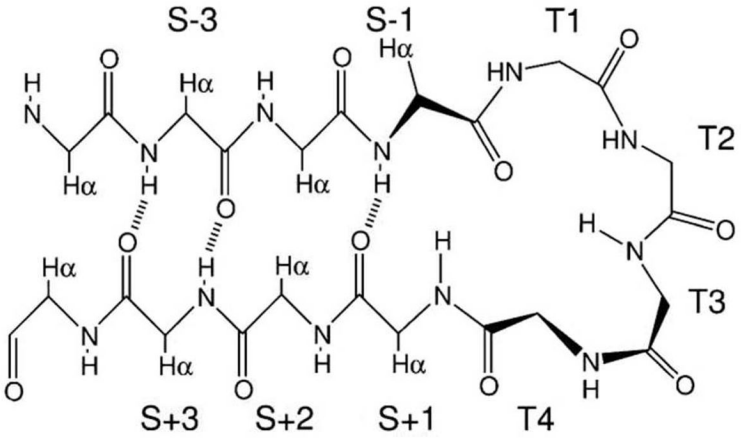

Figure 1.
Nomenclature for HP7-related hairpins.

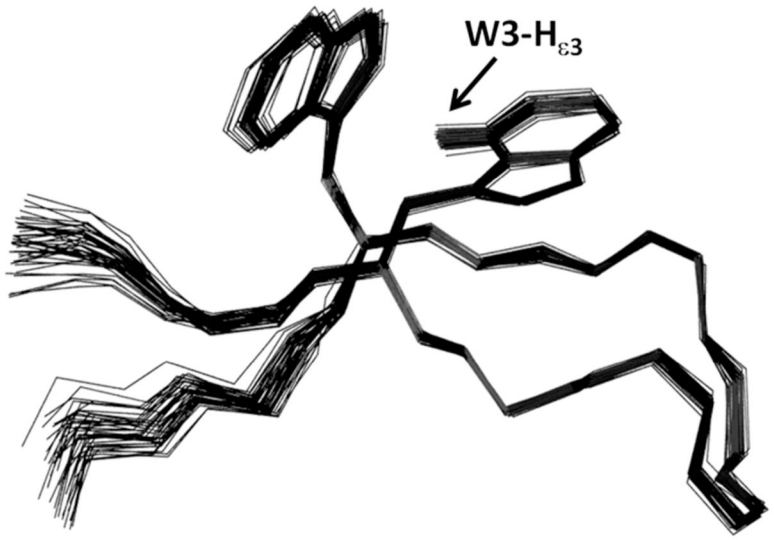

Figure 2.
Packing motif for the turn-flanking indole rings (Trp3 and Trp10) and the backbone conformation of HP7.[63] The W3-Hε3 location is highlighted.

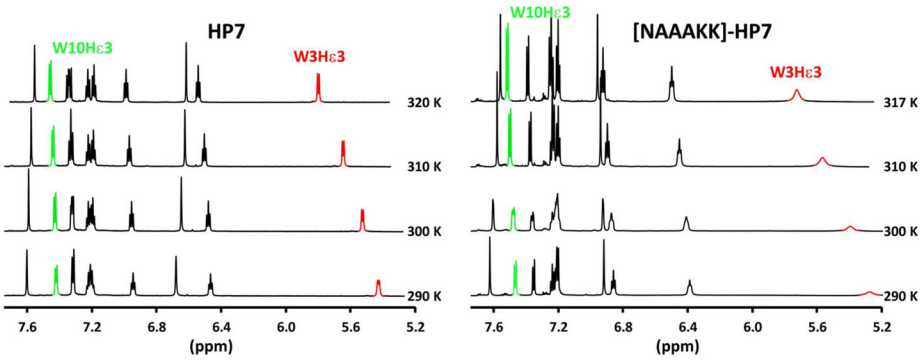

Figure 3.

The aromatic region of 750 MHz NMR spectra of HP7 and a loop region mutant in D_2O (pD 6). The colored peaks are the Hε3 resonances of the two Trp indole rings: red for W3 and green for W10 (which served as the control for no exchange broadening). Even though the NAAAKK loop mutant displays a somewhat larger upfield shift for W3-Hε3 and a comparable shift melt, the extensive line broadening indicates much slower folding dynamics.

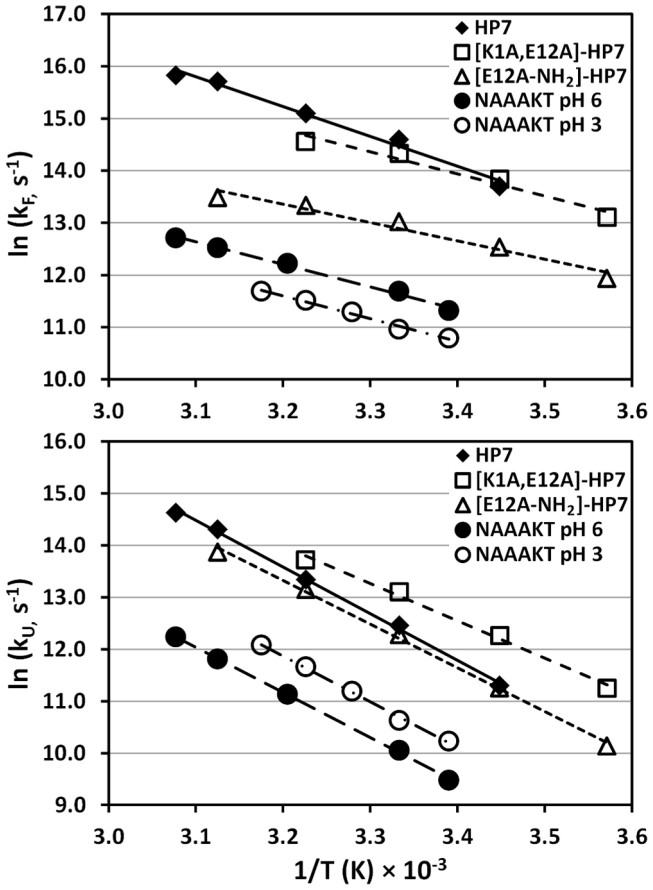

Figure 4.

Arrhenius plots for HP7 (diamonds, ◆), [K1A,E12A]-HP7 (open square, □), [E12A-NH_2]-HP7 (△), and the NAAAKT loop analog at pH 6 (filled circles, ●) and pH 3 (open circles, ○). The folding rate constant plot appears as the top panel. The unfolding rate plots appear in the lower panel. All lines are least squares fits.

Table 1

Representative dynamics data for GB1 hairpin analogs at 297 ± 3 K.

		k_F (10^3/s)	k_U (10^3/s) at 298 K
GB1p	GE WTY-DDATKT-FTV TE	51	179
	D7P	110	90
	K10G	390	780
GB1m2	GE WTY-**NP**AT**GK**-FTV TE	260	156
GB1m3	**KK** WTY-**NP**AT**GK**-FTV **Q**E	520	220
Trpzip4	GE WT**W**-DDATKT-**W**T**W** TE-NH_2	67	4.3 (ref. 36)
HP7	**K**T**W**-**NP**AT**GK**-**W**T**E**	1800	210 (present study)
CLN025	Y**Y**-**DP**ET**G**T-**W**Y	5200	200 (ref. 53)

Table 2

HP7 Mutational Effects on Folding and Unfolding Rates in D_2O.[a]

Mutation	*Temp* (K)	ΔG_U (kJ/mol)	ln k_F	ln k_U
None = KTW-**NPATGK**-WTE	290	5.8	13.7 ± 0.2	11.3 ± 0.2
	300	5.4	14.60	12.46
	320	3.7	15.71	14.31
Strand Mutations				
K1A, E12A [b]	300	3.0	14.33	13.11
E12A-NH_2 [b]	290	3.1	12.54	11.26
	300	1.85	13.02	12.28
	310	0.46	13.33	13.15
Loop Mutations NPATGK →				
DPATGK [b]	300	4.2	14.86	13.18
APATGK [c]	300	−0.95	n. d.	n. d.
N**A**ATGK	300	4.6	14.28	12.41
NPA**A**GK	300 [d]	4.2	13.6 ± 0.3	11.9 ± 0.3
N**A**A**A**GK	300 [d]	6.0	13.1 ± 0.2	10.7 ± 0.2
N**A**A**AKG**	300	1.9	12.18	11.42
N**A**AAKK	300	5.3	11.60	9.47
	310	4.4	12.03	10.34
	317	3.5	12.30	10.97
N**A**A**AKT**	300	4.1	11.69	10.05
	320	1.9	12.52	11.81
at pH 3	300 [e]	0.81	10.96	10.63
	315 [e]	−1.1	11.69	12.08
NPAT**A**K	300	3.8	12.6	11.07
NP**G**TGK	300	3.3	13.7	12.4
N**G**ATGK	280 [d]	4.6	12.13	10.16
	290	4.0	12.51	10.86
N**G**ATGK	300 [d]	2.9	12.88	11.73
N**GG**TGK	280 [d]	2.6	11.24	10.1
	300 [d]	0.17	12.1	12.03
	320 [d]	−2.9	12.6	13.7

[a] Data recorded at nominal pH 6 (750 MHz proton observation) unless otherwise specified. The temperature dependent value used for fully-folded chemical shift of W3-Hε3 was δ_F = 4.98 + 0.005(T-280) except as noted (by [b]). The results using a common temperature invariant 100% folded value (5.10 ppm) appear in the Supporting Information (Table S4).

[b] δ_F = 5.15 + 0.004(T-280) was used for HP7 and related species.

[c] Stability data from ref. 63; dynamics data not available for the same sample.

[d] Measurement made at 500 MHz.

[e] Measurement made at pH 3.